Editors' Suggestion

# Exploring High-Performance *p*-Type Transparent Conducting Oxides Based on Electron Correlation in $V_2O_3$ Thin Films

L. Hu,[1] M.L. Zhao,[2] S. Liang,[3] D.P. Song,[2] R.H. Wei,[1] X.W. Tang,[1] W.H. Song,[1] J.M. Dai,[1]
G. He,[3] C.J. Zhang,[4] X.B. Zhu,[1,*] and Y.P. Sun[1,4,5,†]

[1] *Key Laboratory of Materials Physics, Institute of Solid State Physics, Chinese Academy of Sciences, Hefei 230031, People's Republic of China*

[2] *Department of Physics, Jiangsu University of Science and Technology, Zhenjiang 212003, People's Republic of China*

[3] *School of Physics and Materials Science, Radiation Detection Materials & Devices Lab, Anhui University, Hefei 230601, People's Republic of China*

[4] *High Magnetic Field Laboratory, Chinese Academy of Sciences, Hefei 230031, People's Republic of China*

[5] *Collaborative Innovation Center of Advanced Microstructures, Nanjing 210093, People's Republic of China*

Transparent conducting oxides (TCOs) with the functionality of transparency plus conductivity lie at the center of many technological applications. Commonly used TCOs are *n*-type. However, the performances of *p*-type TCOs lag far behind their *n*-type counterparts and the development of high-performance *p*-type TCOs remains an arduous challenge. The electron correlation due to on-site Coulomb interaction in the correlated metal oxides can not only promote modification of the valence band, which forms the basis for *p*-type conduction, but also shift the screened plasma energy to below the visible region for enhancing optical transparency. In this paper, the electron correlation is utilized as a key material design parameter to improve the performance of *p*-type TCOs. This approach is experimentally verified by decreasing electron correlation from $Cr_2O_3$ to $V_2O_3$, which, despite its high hole concentration ($> 10^{22}$ cm$^{-3}$), has low screened plasma energy (approximately 0.97 eV) and significantly boosts the performance through good balance between the electrical conductivity and optical transparency. These results indicate that the strategy of electron correlation engineering paves an effective way for exploring high-performance *p*-type TCOs in strongly correlated oxides.

## I. INTRODUCTION

Transparent conducting oxides (TCOs), combining the contraindicated properties of high electrical conductivity and high optical transparency, are of great technological interest for a myriad of applications, notably in flat panel displays, photovoltaic cells, touchscreen sensors, and other optoelectronic devices [1–5]. To date, the commonly used TCOs are *n*-type, such as Sn-doped $In_2O_3$ (ITO), Al-doped ZnO (AZO), and F-doped $SnO_2$ (FTO), which are obtained by degenerately doping wide band-gap oxides to realize optimal balance between the electrical conductivity and optical transparency. However, the performances of *p*-type TCOs lag far behind their *n*-type counterparts, which has impeded many of the potential transparent electronic applications from organic and thin-film solar cell designs to the field of transparent electronics [6–10]. This discrepancy stems from the intrinsic electronic structure of metal oxides

that usually possess an oxygen 2*p*-derived valence band (VB) and a conduction band (CB) composed of metal *s* orbitals. Consequently, these *s* orbitals are spatially spread and highly dispersed, facilitating a low (high) electron effective mass (mobility) and excellent electrical conductivity when donor doped. In contrast, the localized nature of oxygen 2*p* orbitals in the VB results in a large (low) hole effective mass (mobility) and poor *p*-type dopability, which becomes the fundamental obstacle to achieving *p*-type TCOs [6,11].

The strategy for reducing the localization behavior is modifying the VB through hybridization of oxygen 2*p* orbitals with the metal *d* or *s* orbitals. Kawazoe *et al.* proposed the concept of "chemical modulation of the valence band" (CMVB) to mitigate this conundrum, which spurs the development of a series of *p*-type TCOs such as Cu-based delafossite oxides and oxychalcogenides [12–23]. Following this design principle, high-throughput material screening has also selected several *p*-type TCOs candidates in view of low hole effective mass and wide band gap to realize high hole mobility and optical

transparency, respectively [24–26]. However, these $p$-type TCOs exhibit imbalance between electrical conductivity and optical transparency, i.e., either low electrical conductivity or high electrical conductivity at the expense of optical transparency, leading to much lower performance as compared to the $n$-type TCOs [6,11]. For example, the Cu-based delafossite oxides are transparent and exhibit $p$-type conductivity; however, their electrical conductivities are usually several orders of magnitude lower than those of $n$-type TCOs arising from the deep level of acceptor defects [27]. Mg-doped CuCrO$_2$ exhibits a high $p$-type conductivity of 220 S cm$^{-1}$ concurrently with a low optical transparency of approximately 30% [15]. The other approach includes utilizing electron correlation produced by strong electron-electron Coulomb interaction $U$ as starting points for exploring $p$-type TCOs. Several transition metal oxides (TMOs) such as NiO, Cr$_2$O$_3$, LaCrO$_3$, LaVO$_3$, Ca$_3$Co$_4$O$_9$, Na$_x$CoO$_2$, Bi$_2$Sr$_2$Co$_2$O$_y$, and Bi$_2$Sr$_2$CaCu$_2$O$_y$ have also been reported as $p$-type TCOs [28–36]. Based on the relative magnitudes of $U$, electronic bandwidth ($W$), and charge-transfer energy between O 2$p$ and $d$ orbitals ($\Delta$), these TMOs can be either Mott insulators (NiO, Cr$_2$O$_3$, LaCrO$_3$, and LaVO$_3$) or $p$-type correlated metals (Ca$_3$Co$_4$O$_9$, Na$_x$CoO$_2$, Bi$_2$Sr$_2$Co$_2$O$_y$, and Bi$_2$Sr$_2$CaCu$_2$O$_y$) [37]. The common feature of their band structures to support $p$-type conduction is that the VB consists of a hybridizing band between the oxygen 2$p$ orbital and the transition metal $d$ orbital or transition metal $d$ orbital driven by the electron correlation [38–41]. From the viewpoint of band structure illustrated by the Hubbard model, the electron correlation splits the $d$ band into the upper Hubbard band (UHB) and lower Hubbard band (LHB), separated by $U$ [37]. As a result, the electronic structure of these TMOs could be modified by the electron correlation. In this regard, the electron correlation plays the same role as CMVB for modification of the VB, which forms the basis for $p$-type conduction.

The strength of electron correlation can be quantified by a renormalization factor $Z_k = m_{band}/m^*$, where $m_{band}$ and $m^*$ are free noninteracting electron effective mass and renormalized electron effective mass incorporating the electron-electron interaction, respectively [42]. In the case of a Mott insulator, all itinerant carriers are localized owing to the electron correlation, which is equivalent to the divergence of $m^*$ ($Z_k = 0$). The effect of electron correlation is determined by the $U/W$ ratio. Decreasing the electron correlation, either by increasing $W$ or decreasing $U$, would increase $Z_k$ and decrease $m^*$, which would result in the increase of the carrier itinerancy and ultimately induce an insulator-to-metal transition (Mott transition) [37]. Recently, Zhang *et al.* have reported that correlated metals of SrVO$_3$ ($Z_k = 0.33$) thin films with high carrier concentrations ($n$) of approximately $10^{22}$ cm$^{-3}$ can be developed as $n$-type TCOs [43]. The design strategy relies on the enhancement of $m^*$ due to electron correlation to

reduce the reflection edge below 1.75 eV, keeping simultaneously a high electrical conductivity ($\sigma$) of approximately $10^4$ S cm$^{-1}$ [43]. Stoner *et al.* used the $Z_k$ as a key material design parameter to optimize the optoelectronic performance of SrMoO$_3$ ($Z_k = 0.48$) thin films as $n$-type TCOs [44].

Besides $n$-type TCOs, the electron correlation could also be used for exploring high-performance $p$-type TCOs. Cr$_2$O$_3$ ($Z_k = 0$), a binary oxide of a Mott insulator belonging to an intermediate case between a Mott-Hubbard insulator and a charge transfer insulator, has been considered as a candidate $p$-type TCO, in which the electron correlation promotes strong hybridization between Cr $t_{2g}$ and O 2$p$ orbitals in the VB [30,39,45,46]. However, the mixed character in the VB of Cr$_2$O$_3$ tends to exhibit the polaronic conduction of holes, resulting in low hole mobility (approximately $10^{-4}$ cm$^2$ V$^{-1}$ s$^{-1}$) and significantly suppress the electrical conductivity [47]. Arca *et al.* demonstrated that VB modification of Cr$_2$O$_3$ by acceptor doping is an effective method to improve its electrical conductivity and performance [46]. In M$_2$O$_3$ ($M = 3d$ transition metal ions), the values of $U$ gradually decrease with the decrease of atomic number of transition metal ions, which affects their electronic structures as well as the resultant electrical properties [48–50]. Therefore, starting from Cr$_2$O$_3$, it is expected that the electrical conductivity can be improved by decreasing $U$ while maintaining the consequence of VB modification due to electron correlation for $p$-type conduction to realize good balance between them. Theoretical calculations based on local density approximation with dynamical mean-field theory (LDA + DMFT) and experimental results have revealed that the $U$ and $Z_k$ values of V$_2$O$_3$ are about 5 eV and 0.12, which satisfy the above requirements [49–51]. As schematically shown in Fig. 1, the decrease of $U$ from Cr$_2$O$_3$ to V$_2$O$_3$ can not only retain the VB modification for $p$-type conduction, but also diminish the hybridization between V $t_{2g}$ and O 2$p$ orbitals to increase the carrier itinerancy (mobility). V$_2$O$_3$ ($Z_k \approx$
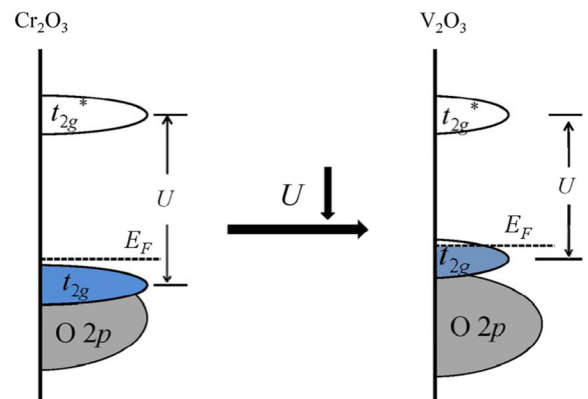


FIG. 1.  Schematic diagram of VB modification due to electron correlation for Cr$_2$O$_3$ and V$_2$O$_3$.

0.12), neighboring to $Cr_2O_3$ with smaller $U$, is a prototypical Mott-Hubbard system showing a metal-to-insulator transition (MIT) at around 155 K from a high-temperature metallic phase to a low-temperature insulating phase [51]. The V $3d$ bands in $V_2O_3$ are split into twofold $e_g$ and threefold $t_{2g}$ bands due to the crystal field. The trigonal distortion of the rhombohedral lattice further degenerates the $t_{2g}$ bands into low-lying doubly degenerate $e_g^\pi$ and nondegenerate $a_{1g}$ bands [52]. In the high-temperature metallic phase of $V_2O_3$, the VB that consists of $e_g^\pi$ and $a_{1g}$ bands is partially occupied by two $t_{2g}$ electrons and the Fermi level is located within the upper VB, which accounts for the $p$-type conduction with high $\sigma$ and $n$ to easily evade the hole doping trouble for most $p$-type TCOs [53–55].

The reflection edge resulting from the fundamental excitation of free carriers occurs at the screened plasma energy $\hbar\omega_p = \hbar(e^2/\epsilon_0\epsilon_r)^{1/2}(n/m^*)^{1/2}$, in which $\hbar$ is the reduced Planck constant, $e$ is the elemental charge, $\varepsilon_0$ is the vacuum permittivity, and $\varepsilon_r$ is the relative permittivity. To open an optical transparency window in the visible spectrum (1.75–3.25 eV), the reflection edge should be below 1.75 eV and the strong interband optical transition should be above 3.25 eV. Therefore, the enhancement of $m^*$ due to electron correlation in the correlated metals of $V_2O_3$ can shift the $\hbar\omega_p$ below 1.75 eV through tuning the $n/m^*$ ratio, which satisfies one of the basic requirements for TCOs [43,44,51]. The optical absorption of $V_2O_3$ in the visible region is attributed to the $d$-$d$ transition from occupied $t_{2g}$ to empty $t_{2g}$ bands, which are moderate in order to not reduce the transparency of the $V_2O_3$ thin films [56]. Accordingly, the strong absorption due to charge transfer excitations from O $2p$ to V $t_{2g}$ bands in the ultraviolet region determines the upper limit of the transparency window ($E_H$) [57]. In general, the high-temperature metallic phase of $V_2O_3$ fulfills all the requirements for $p$-type TCOs based on the criteria of $p$-type conductivity and optical transparency. In this paper, we explore high-performance $p$-type TCOs based on electron correlation in the $V_2O_3$ thin films. The $V_2O_3$ thin films exhibit a high electrical conductivity of 400–2122 S cm$^{-1}$ concurrently with a visible transmittance of 40%–78%. The screened plasma energy stemming from a fundamental excitation of the free carriers is approximately 0.97 eV extracted from the ellipsometry measurements. The $E_H$ is approximately 3.6 eV determined by the strong interband transition from the occupied O $2p$ to the empty V $t_{2g}$ bands. Therefore, the high-performance $p$-type TCOs based on the $V_2O_3$ thin films are obtained by the good balance between the electrical and optical properties.

## II. EXPERIMENT

$V_2O_3$ thin films are grown on $c$-plane $Al_2O_3$ substrates by pulsed laser deposition. A KrF excimer laser ($\lambda = 248$ nm) with a repetition rate of 5 Hz and a laser fluency of 2 J cm$^{-2}$ is focused on a $V_2O_5$ ceramic target. The substrate temperature is kept at 600 °C during the deposition. The films are grown and cooled to room temperature in an Ar atmosphere of 2 Pa. The distance between the target and the substrate is 5 cm. In this growth condition, the growth rate of the $V_2O_3$ thin film is about 6 nm/min. The structural properties of the $V_2O_3$ films are characterized by x-ray diffraction (XRD) using $K_\alpha$ radiation at room temperature. X-ray photoelectron spectroscopy (XPS) with monochromatic Al $K_\alpha$ ($hv = 1486.6$ eV) is used to evaluate the valence states of the elements in an ultrahigh vacuum chamber. Binding energy data are referenced to the C $1s$ peak at 284.8 eV. Electrical transport properties are measured on a physics properties measurement system (PPMS) using the standard four-probe method. Hall measurements are also carried out on PPMS using the van der Pauw geometry. Optical transmission is measured by a UV/Vis/NIR Lambda 900 spectrometer in the wavelength range from 200 to 2000 nm. Room-temperature ellipsometric spectra are collected at an incidence angle of 65° using single rotating-compensator spectroscopic ellipsometers over the infrared to ultraviolet 0.93–4.77 eV.

## III. RESULTS AND DISCUSSION

Figure 2(a) shows the typical XRD pattern of the $V_2O_3$ thin films grown on $c$-plane $Al_2O_3$ substrates. Only (000$l$) peaks for the $V_2O_3$ thin film and $Al_2O_3$ are observed, confirming a single phase and $c$-axis oriented growth of $V_2O_3$. Results for the XRD $\phi$ scan of $V_2O_3$ (10$\bar{1}$4) and $Al_2O_3$ (10$\bar{1}$4) reflections are shown in Fig. 1(b). Threefold symmetry is clearly observed for both the $Al_2O_3$ substrate and $V_2O_3$ thin film due to the same hexagonal structures. This indicates the epitaxial growth of the $V_2O_3$ thin films on the $Al_2O_3$ substrates and the epitaxial relation can be written as (0006) $V_2O_3$ ∥ (0006) $Al_2O_3$ and (1000) $V_2O_3$ ∥ (1000) $Al_2O_3$. The high quality of the $V_2O_3$ thin film is also confirmed by the rock curve scan with the full width at half maximum (FWHM) of 0.09° as shown in the inset of Fig. 1(a).

XPS measurement has been carried out to probe the oxidation state of the $V_2O_3$ thin films. Figure 3(a) displays the spectra of the V $2p$ and O $1s$ core level, in which the dotted and solid lines represent the experimental data and fitting curve, respectively. The V $2p$ level is split into V $2p_{3/2}$ and V $2p_{1/2}$ due to spin-orbital coupling with a separated binding energy of approximately 7.6 eV. The fitting binding energy of V $2p_{3/2}$ is approximately 515.7 eV and the line width of FWHM is approximately 3.4 eV. These values are in good agreement with the previous studies of $V^{3+}$ in $V_2O_3$ [58–60]. The O $1s$ level can be divided into two peaks centered at 530 and 531.1 eV, corresponding to the lattice oxygen ions and the physically adsorbed oxygen at the film surface, respectively [58]. Figure 3(b) presents the XPS spectra of the $V_2O_3$ thin film in the VB region. It
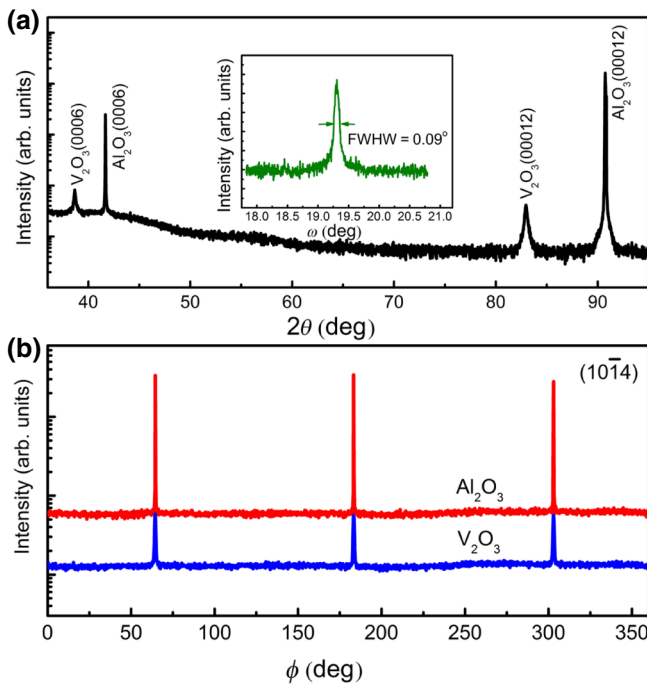
FIG. 2.    (a) XRD $\theta$-$2\theta$ scan of the 56-nm-thick $V_2O_3$ thin film on the $Al_2O_3$ substrate. The inset shows the rocking curve scan of the (0006) diffraction peak of a $V_2O_3$ thin film. (b) XRD $\phi$ scans of $V_2O_3$ $(10\bar{1}4)$ and $Al_2O_3$ $(10\bar{1}4)$ reflections.
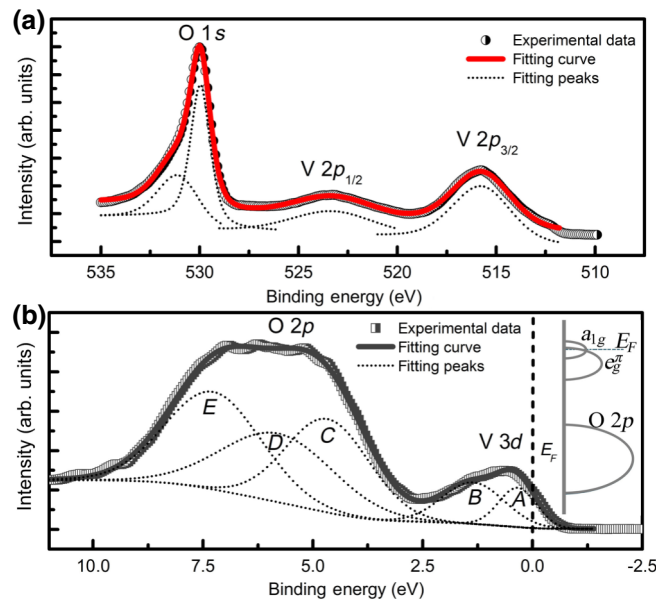


FIG. 3.    (a) XPS spectrum of the V $2p$ and O $1s$ core levels of the $V_2O_3$ thin film. (b) XPS spectra of the $V_2O_3$ thin film in the valence band region. The inset shows the energy level diagram of the $V_2O_3$ thin film in the high-temperature metallic phase.

is found that the spectrum can be assigned to the V $3d$ band ranging from 0 to 2.5 eV and the O $2p$ band in the range of 2.5–9 eV, respectively [53,54,59]. Further analysis indicates that the V $3d$ band consists of A ($a_{1g}$) and B ($e_g^\pi$) bands and the O $2p$ band can be fitted with the C, D, and E peaks, which are consistent with the previous theoretical calculation and experimental results of $V_2O_3$ [50,54,61]. As shown in the inset of Fig. 3(b), the Fermi level $E_F$ lies within the VB formed by the overlapping V ($3d$) $a_{1g}$ and $e_g^\pi$ bands. Accordingly, the $V_2O_3$ clearly exhibits a finite spectral weight at $E_F$, which coincides with the metallic behavior at room temperature.

Figure 4(a) shows the temperature dependence of sheet resistance ($R_S = 1/\sigma t$, $t$ film thickness) for the $V_2O_3$ thin films with different thicknesses. The $V_2O_3$ thin films with thicknesses of 56 and 28 nm exhibit metallic behaviors, in which the decrease of the $R_S$ with decreasing temperature down to approximately 190 K is followed by a weakly insulating behavior. The obvious thermal hysteresis between the cooling and warming processes indicates the first-order nature of the MIT. Nevertheless, the MIT and its accompanied resistance change are broadened and much smaller compared to that of the single crystal, while the resistivity in the high-temperature metallic state is similar with the single crystal [62]. In contrast, the $V_2O_3$ thin films with thicknesses of 14 and 7 nm show insulator-insulator transitions, in which the $R_S$ increases

slowly with decreasing temperature, followed by a rapid increase of approximately 3 orders of magnitude. Previous studies have revealed the coexistence of metallic and insulating phases in the $V_2O_3$ thin films associated with the thermodynamic instability near the transition [63,64].
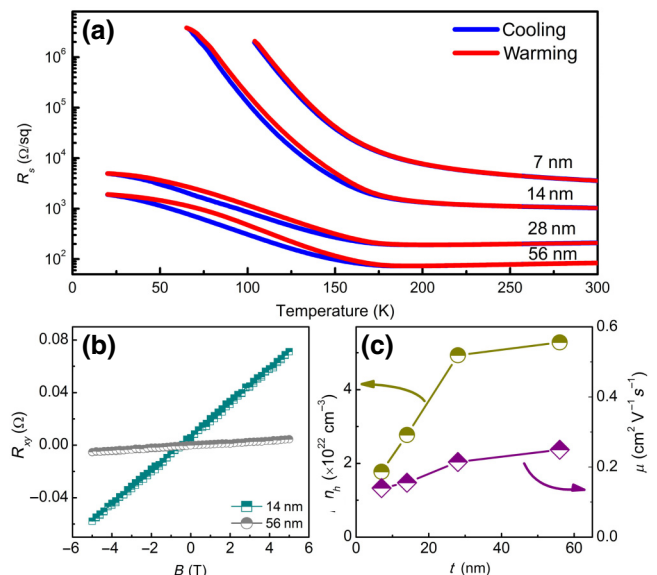


FIG. 4.    (a) Temperature-dependent sheet resistance of the $V_2O_3$ thin films. (b) Evolution of room-temperature Hall resistance with magnetic field. (c) Thickness dependence of room-temperature hole concentration and hole mobility for the $V_2O_3$ thin films.

Furthermore, this instability can be affected by many factors such as strain, substrate disorder, and substrate orientation, which may account for the diverse transport properties observed in the $V_2O_3$ thin films [65–68]. The $R_S$ $(\sigma)$ at room temperature is 3569 (400), 1028 (695), 209 (1704), and 84 (2122) $\Omega$/sq (S cm$^{-1}$) for the 7-, 14-, 28-, and 56-nm $V_2O_3$ thin films, respectively. Figure 3(b) depicts the typical room-temperature Hall resistance versus magnetic field plots for the $V_2O_3$ thin films. The positive Hall coefficients confirm the $p$-type carriers in the $V_2O_3$ thin films. Figure 3(c) shows the derived hole concentration $(n_h)$ and mobility $(\mu)$ for the $V_2O_3$ thin films. The values of $n_h$ $(\mu)$ are in the range of 1.77–5.28 $\times$ 10$^{22}$ cm$^{-3}$ (0.14–0.24 cm$^2$ V$^{-1}$ s$^{-1}$), which is consistent with that in single crystal and thin films [62,69]. The values of $n_h$ in the $V_2O_3$ thin films are the highest among $p$-type TCOs [6,11]. For the $V_2O_3$ ($Z_k \approx 0.12$), the localized V 3$d$ orbital around the VB maximum results in an effective hole mass of $m^* = m_{band}/Z_k \approx 8.3m_{band}$, which would be larger than that of conventional TCOs [24]. The mobility $(\mu)$ is defined as $\mu = e\tau/m^*$, with $\tau$ the scattering time. As a result, the values of $\mu$ would be suppressed by the enhancement of $m^*$ due to strong electron correlation. However, the low $\mu$ can be compensated by the high $n_h$, resulting in high electrical conductivity.

Figure 5 shows optical transmittance of the $V_2O_3$ thin films on $Al_2O_3$ substrates from infrared to ultraviolet regions. The optical transmittance in the visible region $(T)$ is usually quantified by averaging values at wavelengths of 420, 490, 560, 630, and 700 nm including the substrate contribution. The values of $T$ are 78.0%, 72.2%, 54.8%, and 40.0% for the 7, 14, 28, and 56 nm of $V_2O_3$ thin films,

respectively. The inset of Fig. 5 exhibits the photograph of the $V_2O_3$ thin films on a labeled paper. The 7-nm $V_2O_3$ thin film is almost indistinguishable from the $Al_2O_3$ substrate, reflecting the high optical transparency. The $V_2O_3$ thin films become less transparent with increasing film thickness due to the unavoidable optical absorption in the visible region.

To gain a deeper insight into the optical properties for the $V_2O_3$ thin film, the ellipsometry measurements are performed on the $V_2O_3$ thin film $(t = 130$ nm$)$ on a single-side polished $Al_2O_3$ substrate at room temperature. Figure 6 shows the complex dielectric constant $(\epsilon = \epsilon_1 + i\epsilon_2)$ spectra of the $V_2O_3$ thin film extracted from the room-temperature ellipsometry measurements. The dielectric response of the $V_2O_3$ thin film is modeled using combinations of Drude, Lorentz, and Tauc-Lorentz oscillators (see the Supplemental Material [70]). The real part of the dielectric function $(\epsilon_1)$ equals zero at the screened plasma energy $(\hbar\omega_p)$. Therefore, the $\hbar\omega_p$ for the $V_2O_3$ thin film can be determined to be approximately 0.97 eV by setting $\epsilon_1 = 0$, which is consistent with the plasma edge of approximately 1 eV in the $V_2O_3$ single crystal [71]. This value is well below 1.75 eV required for realizing visible optical transparency. The remarkably reduced $\hbar\omega_p$ of the $V_2O_3$ thin film in the metallic phase with a high carrier concentration is a direct consequence of the enhancement of $m^*$ due to strong electron correlation, which is similar to that in the correlated metals of $SrVO_3$ and $SrMoO_3$ [43,44]. Furthermore, the values of $\epsilon_2$ intimately tied to the optical absorption in the visible region are relatively moderate, which is also important for the realization of high optical transparency in thin-film materials to reduce absorption. The $\epsilon_2$ increases in the infrared region due to the free-carrier excitation.
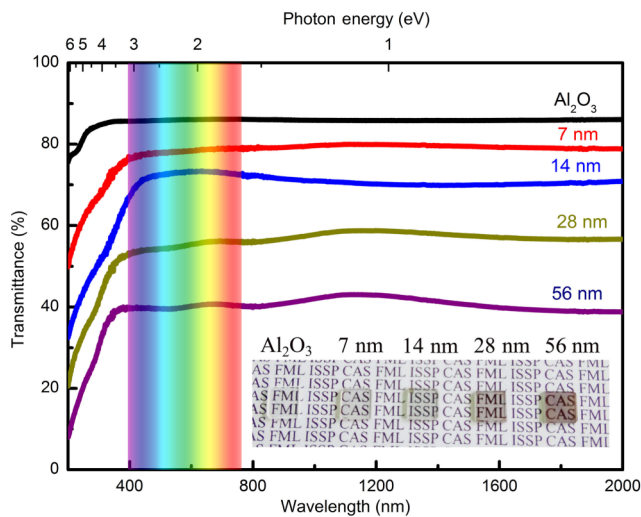


FIG. 5. (a) Optical transmittance spectra for the $Al_2O_3$ substrate and $V_2O_3$ thin films with different thicknesses. The range of the visible spectrum is illustrated. The inset shows the photographs of the $Al_2O_3$ substrate and $V_2O_3$ thin films with different thicknesses on the $V_2O_3$ substrates.

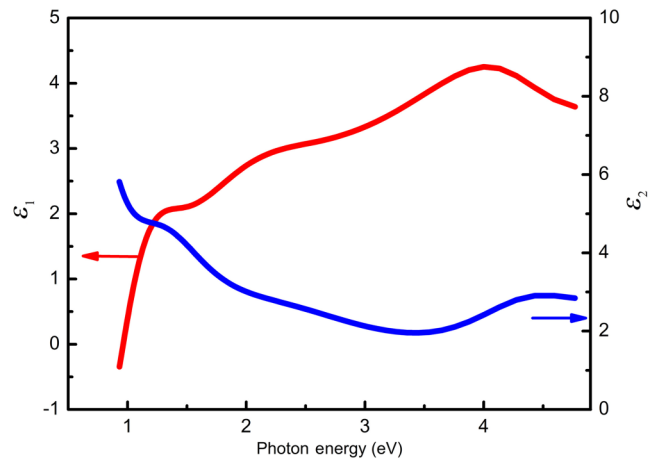

FIG. 6. Complex dielectric function $(\epsilon = \epsilon_1 + i\epsilon_2)$ spectra of the $V_2O_3$ thin film $(t = 130$ nm$)$ extracted from room-temperature spectroscopic ellipsometry measurements.
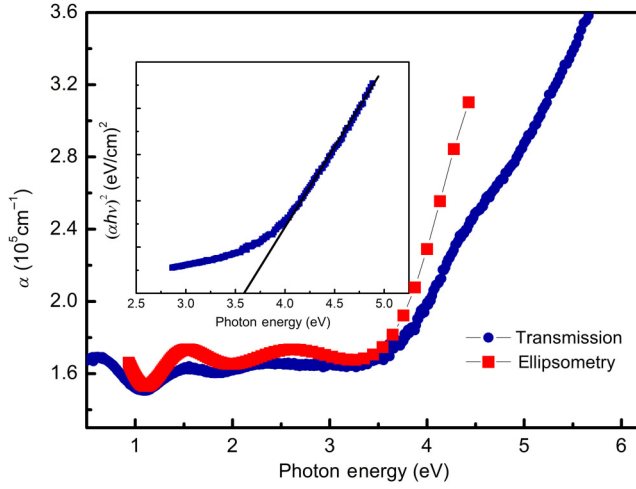
FIG. 7. Optical absorption coefficients for the $V_2O_3$ thin film derived from transmission ($t = 56$ nm) and ellipsometry measurements ($t = 130$ nm), respectively. The inset shows the Tauc plot to estimate $E_H$.
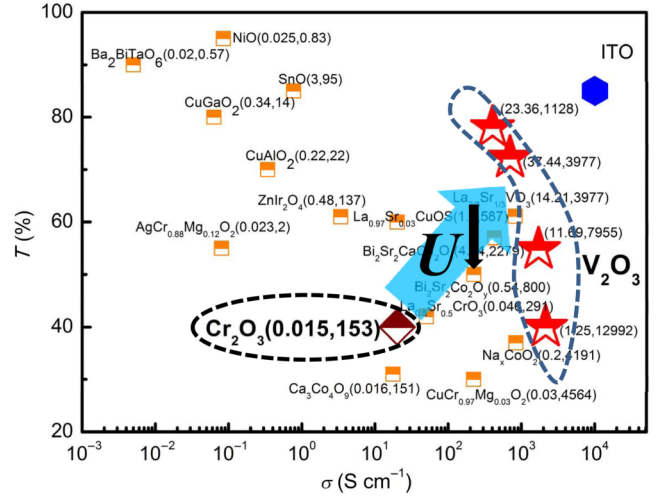


FIG. 8. Graphical representation of $T$ and $\sigma$ for the $V_2O_3$ thin films (red semisolid stars) and other typical *p*-type TCOs. The numbers in parentheses show the corresponding values of $F^H$ and $F^G$ in the units of $M\Omega^{-1}$. The *n*-type TCO of ITO thin film is also added for comparison. The blue arrow indicates the enhancement of performance through electron correlation engineering.

Another important parameter for the optical transparency window in the visible spectrum is the upper limit of the transparency window ($E_H$), above which the material is obscure for the incident photon [57]. Usually, the $E_H$ is determined by the strong optical absorption due to the direct interband transition. Figure 7 shows the experimental absorption spectra for the $V_2O_3$ thin film derived from transmission and ellipsometry measurements, respectively. The absorption coefficient ($\alpha$) spectra can be calculated using the equation of $\alpha = 4\pi\kappa/\lambda$, where $\lambda$ is the wavelength and $\kappa$ is the extinction coefficient. The relationship between $\kappa$ and the dielectric constant is

$$\kappa = \sqrt{\left(\sqrt{\epsilon_1^2 + \epsilon_2^2} - \epsilon_1\right)/2}.$$ It is clear that the optical absorption features of the $V_2O_3$ thin film can be well extracted from both the transmission and ellipsometry spectra. The low-intensity spectral features observed in the 1.0–3.5 eV range can be assigned as the $t_{2g}$-$t_{2g}$ interband transitions [56,72]. A strong absorption edge is observed at the photon energy of approximately 4.0 eV due to the interband transition from the O $2p$ to the empty V $t_{2g}$ bands. $E_H$ can be determined by fitting the absorption edge through the Tauc relation, $(\alpha h v)^2 = C(h v - E_H)$, where $h v$ is the photon energy and $C$ is a constant. As shown in the inset of Fig. 7, the linear fitting yields an $E_H$ of approximately 3.6 eV, which is well above 3.25 eV for visible transparency.

Figure 8 illustrates $T$ and $\sigma$ for the $V_2O_3$ thin films (red semisolid stars) and other typical *p*-type TCOs. The $\sigma$ of *p*-type TCOs are distributed over a wide range of several orders of magnitude. It is well known that the practical applications of the *p*-type TCOs rely on simultaneously high $T$ and $\sigma$. Clearly, the $V_2O_3$ thin film becomes a front

runner in the pursuit of high-performance *p*-type TCOs due to the good balance between electrical and optical properties. It is convenient to quantitatively evaluate the performance of *p*-type TCOs by a figure of merit (FOM). Two types of FOM are often calculated by $F^H = T^{10}/R_S$ and $F^G = -1/(R_S \ln T)$, which were proposed by Haacke and Gordon, respectively [73,74]. The larger values of FOM indicate higher performances of the TCOs. However, $F^H$ overestimates the contribution of $R_S$, while $F^G$ overestimates the importance of $T$. Therefore, both $F^H$ and $F^G$ should be considered simultaneously to yield a fair evaluation of the performance of *p*-type TCOs. The numbers in parentheses show the corresponding values of $F^H$ and $F^G$ in the units of $M\Omega^{-1}$ for the $V_2O_3$ thin films and other reported *p*-type TCOs (also in Table S2 in the Supplemental Material [70]). In particular, it should be noted that the performance of *p*-type TCOs can be remarkably enhanced in the $M_2O_3$ compounds from $Cr_2O_3$ to $V_2O_3$. The decrease of $U$ would be the main driving force. This result indicates that the strategy of electron correlation engineering paves an effective way for exploring high-performance *p*-type TCOs in strongly correlated oxides.

## IV. CONCLUSION

In summary, we demonstrate that the correlated metallic phase of $V_2O_3$ thin films can be explored as *p*-type TCOs with high performance. The electron correlated-driven VB engineering in $V_2O_3$ forms the basis for *p*-type conduction. The intrinsic metallic phase of $V_2O_3$ with high carrier

concentration ($> 10^{22}$ cm$^{-3}$) guarantees its high electrical conductivity. Combining low screened plasma energy (approximately 0.97 eV) and moderate absorption in the visible region, the $V_2O_3$ thin films exhibit the visible transmittances of 40%–78%. These results indicate that the $V_2O_3$ thin films can be developed as a high-performance *p*-type TCO and provide an alternative route to explore high-performance *p*-type TCOs in strongly correlated oxides. Furthermore, the $V_2O_3$ thin films as high-performance *p*-type TCOs can be potentially used in several transparent device applications such as rectifiers, photodetectors, and solar cells [6,75].

[1] K. Ellmer, Past achievements and future challenges in the development of optically transparent electrodes, Nat. Photonics **6**, 809 (2012).

[2] C. G. Granqvist, Transparent conductors as solar energy materials: A panoramic review, Sol. Energy Mater. Sol. Cells **91**, 1529 (2007).

[3] E. Fortunato, D. Ginley, H. Hosono, and D. C. Paine, Transparent conducting oxides for photovoltaics, MRS Bull. **32**, 242 (2007).

[4] E. Fortunato, P. Barquinha, and R. Martins, Oxide semiconductor thin-film transistors: A review of recent advances, Adv. Mater. **24**, 2945 (2012).

[5] T. Minami, Transparent conducting oxide semiconductors for transparent electrodes, Semicond. Sci. Technol. **20**, S35 (2005).

[6] Z. Wang, P. K. Nayak, J. A. Caraveo-Frescas, and H. N. Alshareef, Recent developments in *p*-type oxide semiconductor materials and devices, Adv. Mater. **28**, 3831 (2016).

[7] W. Beyer, J. Hupkes, and H. Stiebig, Transparent conducting oxide films for thin film silicon photovoltaics, Thin Solid Films **516**, 147 (2007).

[8] H. Ohta and H. Hosono, Transparent oxide optoelectronics, Mater. Today **3**, 42 (2004).

[9] H. Kawazoe, H. Yanagi, and K. Ueda, Transparent *p*-type conducting oxides: Design and fabrication of *p-n* heterojunctions, MRS Bull. **25**, 28 (2000).

[10] A. Banerjee and K. Chattopadhyay, Recent developments in the emerging field of crystalline *p*-type transparent conducting oxide thin films, Prog. Cryst. Growth Charact. Mater. **50**, 52 (2005).

[11] K. H. L. Zhang, K. Xi, M. Blamire, and R. G. Egdell, *P*-type transparent conducting oxides, J. Phys.: Condens. Matter **28**, 383002 (2016).

[12] H. Kawazoe, M. Yasukawa, H. Hyodo, M. Kurita, H. Yanagi, and H. Hosono, *P*-type electrical conduction in transparent thin films of CuAlO$_2$, Nature **389**, 939 (1997).

[13] H. Yanagi, S. Inoue, K. Ueda, H. Kawazoe, H. Hosono, and N. Hamada, Electronic structure and optoelectronic properties of transparent *p*-type conducting CuAlO$_2$, J. Appl. Phys. **88**, 4159 (2000).

[14] K. Ueda, T. Hase, H. Yanagi, H. Kawazoe, H. Hosono, H. Ohta, M. Orita, and M. Hirano, Epitaxial growth of transparent *p*-type conducting CuGaO$_2$ thin films on sapphire (001) substrates by pulsed laser deposition, J. Appl. Phys. **89**, 1790 (2001).

[15] R. Nagarajan, A. D. Draeseke, A. W. Sleight, and J. Tate, *p*-type conductivity in CuCr$_{1-x}$Mg$_x$O$_2$ films and powders, J. Appl. Phys. **89**, 8022 (2001).

[16] N. Duan, A. W. Sleight, M. K. Jayaraj, and J. Tate, Transparent *p*-type conducting CuScO$_{2+x}$ films, Appl. Phys. Lett. **77**, 1325 (2000).

[17] M. Marquardt, N. Ashmore, and D. P. Cann, Crystal chemistry and electrical properties of the delafossite structure, Thin Solid Films **496**, 146 (2006).

[18] A. Kudo, H. Yanagi, H. Hosono, and H. Kawazoe, SrCu$_2$O$_2$: A *p*-type conductive oxide with wide band gap, Appl. Phys. Lett. **73**, 220 (1998).

[19] E. Fortunato, R. Barros, P. Barquinha, V. Figueiredo, S. K. Park, C. Hwang, and R. Martins, Transparent *p*-type SnO$_x$ thin film transistors produced by reactive rf magnetron sputtering followed by low temperature annealing, Appl. Phys. Lett. **97**, 052105 (2010).

[20] M. Dekkers, G. Rijnders, and D. H. A. Blank, ZnIr$_2$O$_4$, a *p*-type transparent oxide semiconductor in the class of spinel zinc-*d*$^6$-transition metal oxide, Appl. Phys. Lett. **90**, 021903 (2007).

[21] R. H. Wei, X. W. Tang, L. Hu, Z. Z. Hui, J. Yang, H. M. Luo, X. Luo, J. M. Dai, W. H. Song, Z. R. Yang, X. B. Zhu, and Y. P. Sun, Facile chemical solution synthesis of *p*-type delafossite Ag-based transparent conducting AgCrO$_2$ films in an open condition, J. Mater. Chem. C **5**, 1885 (2017).

[22] H. Hiramatsu, K. Ueda, H. Ohta, M. Hirano, M. Kikuchi, H. Yanagi, T. Kamiya, and H. Hosono, Heavy hole doping of epitaxial thin films of a wide gap *p*-type semiconductor, LaCuOSe, and analysis of the effective mass, Appl. Phys. Lett. **91**, 012104 (2007).

[23] H. Hiramatsu, K. Ueda, H. Ohta, M. Orita, M. Hirano, and H. Hosono, Preparation of transparent *p*-type (La$_{1-x}$Sr$_x$O)CuS thin films by r.f. sputtering technique, Thin Solid Films **411**, 125 (2002).

[24] G. Hautier, A. Miglio, G. Ceder, G. Rignanese, and X. Gonze, Identification and design principles of low hole effective mass *p*-type transparent conducting oxides, Nat. Commun. **4**, 2292 (2013).

[25] N. Sarmadian, R. Saniz, B. Partoens, and D. Lamoen, Easily doped *p*-type, low hole effective mass, transparent oxides, Sci. Rep. **6**, 20446 (2016).

[26] A. Bhatia, G. Hautier, T. Nilgianskul, A. Miglio, J. Sun, H. J. Kim, K. H. Kim, S. Chen, G. Rignanese, X. Gonze, and J. Suntivich, High-mobility bismuth-based transparent

*p*-type oxide from high-throughput material screening, Chem. Mater. **28**, 30 (2016).

[27] J. Tate, H. L. Ju, J. C. Moon, A. Zakutayev, A. P. Richard, J. Russell, and D. H. McIntyre, Origin of *p*-type conduction in single-crystal CuAlO$_2$, Phys. Rev. B **80**, 165206 (2009).

[28] H. Sato, T. Minami, S. Takata, and T. Yamada, Transparent conducting *p*-type NiO thin films prepared by magnetron sputtering, Thin Solid Films **236**, 27 (1993).

[29] P. Zhai, Q. Yi, J. Jian, H. Wang, P. Song, C. Dong, X. Lu, Y. Sun, J. Zhao, X. Dai, Y. Lou, H. Yang, and G. Zou, Transparent *p*-type epitaxial thin films of nickel oxide, Chem. Commun. **50**, 1854 (2014).

[30] E. Arca, K. Fleischer, and I. V. Shvets, Magnesium, nitrogen codoped Cr$_2$O$_3$: A *p*-type transparent conducting oxide, Appl. Phys. Lett. **99**, 111910 (2011).

[31] K. H. L. Zhang, Y. Du, A. Papadogianni, O. Bierwagen, S. Sallis, L. F. J. Piper, M. E. Bowden, V. Shutthanandan, P. V. Sushko, and S. A. Chambers, Perovskite Sr-doped LaCrO$_3$ as a new *p*-type transparent conducting oxide, Adv. Mater. **27**, 5191 (2015).

[32] L. Hu, R. H. Wei, J. Yan, D. Wang, X. W. Tang, X. Luo, W. H. Song, J. M. Dai, X. B. Zhu, C. J. Zhang, and Y. P. Sun, La$_{2/3}$Sr$_{1/3}$VO$_3$ thin films: A new *p*-type transparent conducting oxide with very high figure of merit, Adv. Electron. Mater. **4**, 1700476 (2018).

[33] M. Aksit, S. K. Kolli, I. M. Slauch, and R. D. Robinson, Misfit layered Ca$_3$Co$_4$O$_9$ as a high figure of merit *p*-type transparent conducting oxide film through solution processing, Appl. Phys. Lett. **104**, 161901 (2014).

[34] D. C. Yuan, J. L. Wang, N. Fu, X. L. Wu, Y. J. Ma, and S. F. Wang, Transparent conducting properties of *c*-axis-oriented Na$_x$CoO$_2$ epitaxial thin films, Sci. China-Phys. Mech. Astron. **61**, 107321 (2018).

[35] R. H. Wei, X. W. Tang, L. Hu, Z. Z Hui, J. Yang, H. M. Luo, X. Luo, J. M. Dai, w. H. Song, Z. R. Yang, X. B. Zhu, and Y. P. Sun, Transparent conducting *p*-type thin films of *c*-axis self-oriented Bi$_2$Sr$_2$Co$_2$O$_y$ with high figure of merit, Chem. Commun. **50**, 9697 (2014).

[36] R. H. Wei, L. Zhang, L. Hu, X. W. Tang, J. Yang, J. M. Dai, W. H. Song, X. B. Zhu, and Y. P. Sun, *p*-type transparent conductivity in high temperature superconducting Bi-2212 thin films, Appl. Phys. Lett. **112**, 251109 (2018).

[37] M. Imada, A. Fujimori, and Y. Tokura, Metal-insulator transitions, Rev. Mod. Phys. **70**, 1039 (1998).

[38] J. Y. Zhang, W. W. Li, R. L. Z. Hoye, J. L. MacManus-Driscoll, M. Budde, O. Bierwagen, L. Wang, Y. Du, M. J. Wahila, L. F. J. Piper, T.-L. Lee, H. J. Edwards, V. R. Dhanak, and K. H. L. Zhang, Electronic and transport properties of Li-doped NiO epitaxial thin films, J. Mater. Chem. C **6**, 2275 (2018).

[39] A. B. Kehoe, E. Arca, D. O. Scanlon, I. V. Shvets, and G. W. Watson, Assessing the potential of Mg-doped Cr$_2$O$_3$ as a novel *p*-type transparent conducting oxide, J. Phys.: Condens. Matter **28**, 125501 (2016).

[40] Z. Q. Yang, Z. Huang, L. Ye, and X. D. Xie, Influence of parameters U and J in the LSDA + U method on electronic structure of the perovskites LaMO$_3$ (*M* = Cr, Mn, Fe, Co, Ni), Phys. Rev. B **60**, 15674 (1999).

[41] T. Takeuchi, T. Kondo, T. Takami, H. Takahashi, H. Ikuta, U. Mizutani, K. Soda, R. Funahashi, M. Shikano, M. Mikami, S. Tsuda, T. Yokoya, S. Shin, and T. Muro, Contribution of electronic structure to the large thermoelectric power in layered cobalt oxides, Phys. Rev. B **69**, 125410 (2004).

[42] D. N. Basov, R. D. Averitt, D. van der Marel, M. Dressel, and K. Haule, Electrodynamics of correlated electron materials, Rev. Mod. Phys. **83**, 471 (2011).

[43] L. Zhang, Y. Zhou, L. Guo, W. Zhao, A. Barnes, H.-T. Zhang, C. Eaton, Y. Zheng, M. Brahlek, H. F. Haneef, N. J. Podraza, M. H. W. Chan, V. Gopalan, K. M. Rabe, and R. Engel-Herbert, Correlated metals as transparent conductors, Nat. Mater. **15**, 204 (2016).

[44] J. L. Stoner, P. A. E. Murgatroyd, M. O'Sullivan, M. S. Dyer, T. D. Manning, J. B. Claridge, M. J. Rosseinsky, and J. Alaria, Chemical control of correlated metals as transparent conductors, Adv. Funct. Mater. **29**, 1808609 (2019).

[45] F. Lebreau, M. M. Islam, B. Diawara, and P. Marcus, Structural, magnetic, electronic, defect, and diffusion properties of Cr$_2$O$_3$: A DFT + U study, J. Phys. Chem. C **118**, 18133 (2014).

[46] E. Arca, A. B. Kehoe, T. D. Veal, A. Shmeliov, D. O. Scanlon, C. Downing, D. Daly, D. Mullarkey, I. V. Shvets, V. Nicolosi, and G. W. Watson, Valence band modification of Cr$_2$O$_3$ by Ni-doping: Creating a high figure of merit *p*-type TCO, J. Mater. Chem. C **5**, 12610 (2017).

[47] L. Farrell, K. Fleischer, D. Caffrey, D. Mullarkey, E. Norton, and I. V. Shvets, Conducting mechanism in the epitaxial *p*-type transparent conducting oxide Cr$_2$O$_3$ : Mg, Phys. Rev. B **91**, 125202 (2015).

[48] T. Uozumi, K. Okada, A. Kotani, R. Zimmermann, P. Steiner, S. Hufner, Y. Tezuka, and S. Shin, Theoretical and experimental studies on the electronic structure of M$_2$O$_3$ (*M* = Ti, V, Cr, Mn, Fe) compounds by systematic analysis of high-energy spectroscopy, J. Electron. Spectrosc. Relat. Phenom. **83**, 9 (1997).

[49] K. Held, G. Keller, V. Eyert, D. Vollhardt, and V. I. Anisimov, Mott-Hubbard Metal-insulator Transition in Paramagnetic V$_2$O$_3$: An LDA + DMFT(QMC) Study, Phys. Rev. Lett. **86**, 5345 (2001).

[50] G. Keller, K. Held, V. Eyert, D. Vollhardt, and V. I. Anisimov, Electronic structure of paramagnetic V$_2$O$_3$: Strongly correlated metallic and Mott insulating phase, Phys. Rev. B **70**, 205116 (2004).

[51] M. K. Stewart, D. Brownstead, S. Wang, K. G. West, J. G. Ramirez, M. M. Qazilbash, N. B. Perkins, I. K. Schuller, and D. N. Basov, Insulator-to-metal transition and correlated metallic state of V$_2$O$_3$ investigated by optical spectroscopy, Phys. Rev. B **85**, 205113 (2012).

[52] F. Rodolakis, J.-P. Rueff, M. Sikora, I. Alliot, J.-P. Itie, F. Baudelet, S. Ravy, P. Wzietek, P. Hansmann, A. Toschi, M. W. Haverkort, G. Sangiovanni, K. Held, P. Metcalf, and M. Marsi, Evolution of the electronic structure of a Mott system across its phase diagram: X-ray absorption spectroscopy study of (V$_{1−x}$Cr$_x$)$_2$O$_3$, Phys. Rev. B **84**, 245113 (2011).

[53] E. Papalazarou, M. Gatti, M. Marsi, V. Brouet, F. Iori, L. Reining, E. Annese, I. Vobornik, F. Offi, A. Fondacaro, S. Huotari, P. Lacovig, O. Tjernberg, N. B. Brookes, M. Sacchi, P. Metcalf, and G. Panaccione, Valence-band electronic

structure of $V_2O_3$: Identification of V and O bands, Phys. Rev. B **80**, 155115 (2009).

[54] S. S. Majid, D. K. Shukla, F. Rahman, K. Gautam, R. J. Choudhary, V. G. Sathe, and D. M. Phase, Stabilization of metallic phase in $V_2O_3$ thin film, Appl. Phys. Lett. **110**, 173101 (2017).

[55] I. Lo Vecchio, L. Baldassarre, F. Dapuzzo, O. Limaj, D. Nicoletti, A. Perucchi, L. Fan, P. Metcalf, M. Marsi, and S. Lupi, Optical properties of $V_2O_3$ in its whole phase diagram, Phys. Rev. B **91**, 155133 (2015).

[56] S. E. Chamberlin, I. H. Nayyar, T. C. Kaspar, P. V. Sushko, and S. A. Chambers, Electronic structure and optical properties of $\alpha$-$(Fe_{1-x}V_x)_2O_3$ solid-solution thin films, Appl. Phys. Lett. **106**, 041905 (2015).

[57] K. R. Eppelmeier and J. M. Rondinelli, Correlated oxides: Metals amassing transparency, Nat. Mater. **15**, 132 (2016).

[58] S. Autier-Laurent, B. Mercey, D. Chippaux, P. Limelette, and Ch. Simon, Strain-induced pressure effect in pulsed laser deposited thin films of the strongly correlated oxide $V_2O_3$, Phys. Rev. B **74**, 195109 (2006).

[59] E. Hryha, E. Rutqvist, and L. Nyborg, Stoichiometric vanadium oxides studied by XPS, Surf. Interface Anal. **44**, 1022 (2012).

[60] X. B. Liu, H. B. Lu, M. He, K. J. Jin, and G. Z. Yang, Room-temperature epitaxial growth of $V_2O_3$ films, Sci. China-Phys. Mech. Astron. **57**, 1866 (2014).

[61] R. L. Kurtz and V. E. Henrich, Surface electronic structure and chemisorption on corundum transition-metal oxides: $V_2O_3$, Phys. Rev. B **28**, 6699 (1983).

[62] D. B. McWhan and J. P. Remeika, Metal-insulator transition in $(V_{1-x}Cr_x)_2O_3$, Phys. Rev. B **2**, 3734 (1970).

[63] S. Lupi *et al.*, A microscopic view on the Mott transition in chromium-doped $V_2O_3$, Nat. Commun. **1**, 105 (2010).

[64] A. S. McLeod, E. van Heumen, J. G. Ramirez, S. Wang, T. Saerbeck, S. Guenon, M. Goldflam, L. Anderegg, P. Kelly, A. Mueller, M. K. Liu, K. Schuller Ivan, and D. N. Basov, Nanotextured phase coexistence in the correlated insulator $V_2O_3$, Nat. Phys. **13**, 80 (2016).

[65] Q. Luo, Q. Guo, and E. G. Wang, Thickness-dependent metal–insulator transition in $V_2O_3$ ultrathin films, Appl. Phys. Lett. **84**, 2337 (2004).

[66] B. S. Allimi, M. Aindow, and S. P. Alpay, Thickness dependence of electronic phase transitions in epitaxial $V_2O_3$ films on (0001) $LiTaO_3$, Appl. Phys. Lett. **93**, 112109 (2008).

[67] J. Brockman, M. G. Samant, K. P. Roche, and S. S. P. Parkin, Substrate-induced disorder in $V_2O_3$ thin films grown on annealed $c$-plane sapphire substrates, Appl. Phys. Lett. **101**, 051606 (2012).

[68] J. Sakai, P. Limelette, and H. Funakubo, Transport properties and $c/a$ ratio of $V_2O_3$ thin films grown on C- and R-plane sapphire substrates by pulsed laser deposition, Appl. Phys. Lett. **107**, 241901 (2015).

[69] C. Grygiel, Ch. Simon, B. Mercey, W. Prellier, R. Fresard, and P. Limelette, Thickness dependence of the electronic properties in $V_2O_3$ thin films, Appl. Phys. Lett. **91**, 262103 (2007).

[70] See the Supplemental Material at http://link.aps.org/supplemental/10.1103/PhysRevApplied.12.044035 for the spectroscopic ellipsometry measurement and modeling of the $V_2O_3$ thin film. Also, the performances of reported $p$-type TCOs in the literature and the $V_2O_3$ thin films are given.

[71] A. S. Barker and J. P. Remeika, Optical properties of $V_2O_3$ doped with chromium, Solid State Commun. **8**, 1521 (1970).

[72] M. M. Qazilbash, A. A. Schafgans, K. S. Burch, S. J. Yun, B. G. Chae, B. J. Kim, H. T. Kim, and D. N. Basov, Electrodynamics of the vanadium oxides $VO_2$ and $V_2O_3$, Phys. Rev. B **77**, 115121 (2008).

[73] C. Haacke, New figure of merit for transparent conductors, J. Appl. Phys. **47**, 4086 (1976).

[74] R. G. Gordon, Criteria for choosing transparent conductors, MRS Bull. **25**, 52 (2000).

[75] C. Chen, T. Wei, P. Hsiao, and C. Hung, Vanadium oxide as transparent carrier-selective layer in silicon hybrid solar cells promoting photovoltaic performances, ACS Appl. Energy Mater. **2**, 4873 (2019).